Lab on a Chip

Cite this: *Lab Chip*, 2012, **12**, 2438–2451

www.rsc.org/loc

FOCUS

Acoustofluidics 14: Applications of acoustic streaming in microfluidic devices

Martin Wiklund,*[a] Roy Green*[b] and Mathias Ohlin[a]

DOI: 10.1039/c2lc40203c

In part 14 of the tutorial series "*Acoustofluidics – exploiting ultrasonic standing wave forces and acoustic streaming in microfluidic systems for cell and particle manipulation*", we provide a qualitative description of acoustic streaming and review its applications in lab-on-a-chip devices. The paper covers boundary layer driven streaming, including Schlichting and Rayleigh streaming, Eckart streaming in the bulk fluid, cavitation microstreaming and surface-acoustic-wave-driven streaming.

[a]*Department of Applied Physics, Royal Institute of Technology, KTH-Albanova, SE-106 91 Stockholm, Sweden. E-mail: martin@biox.kth.se*
[b]*School of Engineering Sciences, University of Southampton, Southampton, SO17 1BJ, United Kingdom. E-mail: R.Green@soton.ac.uk*

I Introduction

Acoustic streaming is a well-known phenomenon within the acoustics community. However, due to the many forms in which it may arise, it is often misunderstood outside of the relatively small circle of researchers actively involved in its study. As well as being misunderstood, acoustic streaming is also often seen in a bad light because of the inadvertent generation of streaming flows inside many acoustically driven microfluidics devices. Whilst it is undeniable that acoustic streaming can be a problematic phenomenon, when used correctly it can be an extremely useful phenomenon that makes it possible to overcome many of the challenges presented by low Reynolds number flows in microfluidics.

Broadly speaking, acoustic streaming can be regarded as any flow generated by the force arising from the presence of a gradient in the time-averaged acoustic momentum flux in a fluid.[1] Within the next few pages it will become clearer what is meant by this but for the time being we shall suffice with a less explicit definition of acoustic streaming as a fluid flow generated by the attenuation of an

Martin Wiklund

Martin Wiklund is Associate Professor in applied physics at the Dept. of Applied Physics, Royal Institute of Technology (KTH), Stockholm, Sweden. He received his M.Sc. in engineering physics from Lund University in 1999 and his Ph.D. in physics from the Dept. of Physics, KTH, Stockholm, in 2004. In 2004–2005, he was postdoctoral fellow at the Fraunhofer Institute for Biomedical Engineering (IBMT), Berlin, Germany. He returned to KTH in 2005, becoming an Assistant Professor in 2006, and Associate Professor in 2009. Currently, Wiklund's research is focused on acoustic and optical methods for micro-scaled handling and characterization of cells, and applications of the methods to biomedical research. He is also a lecturer in various courses in basic physics, optics, ultrasound physics and diagnostic ultrasound. He is author of >20 peer-reviewed journal papers, >50 conference contributions including >20 invited talks, two patents and a recent book chapter ("Ultrasonic Manipulation of Single Cells", In: Single-Cell Analysis: Methods and Protocols, Methods in Molecular Biology, vol. 853, Springer, 2012).

Foreword

In this fourteenth paper in the Lab on a chip tutorial series of Acoustofluidics, Martin Wiklund, Roy Green and Mathias Ohlin discuss applications of acoustic streaming in microfluidic devices. The applications can be divided into two groups, the first one aiming at suppressing the streaming phenomena as in standing wave particle manipulation, the other one utilizing the acoustic streaming with fluid mixing as an example. Different aspects of streaming are covered, such as Rayleigh streaming and Eckart streaming, as well as cavitation microstreaming and SAW induced streaming.

Andreas Lenshof – coordinator of the Acoustofluidics series

acoustic wave. The first theoretical model to thoroughly describe acoustic streaming flows was derived by Rayleigh in 1884.[2] Within his paper, Rayleigh treats three cases of streaming observed experimentally by Faraday and Dvorak. The first two cases relate to the observations made by Faraday[3] on the patterns assumed by sand and fine powders on Chladni's vibrating plates.[4] The third case relates to the observations made by Dvorak[5] on the circulation of air currents in a Kundt's tube. To date, there has been a large quantity of literature published on the topic of acoustic streaming including both analytical and numerical models, experimental studies and, more recently, the application of acoustic streaming to existing problems within microfluidics.

The aim of this tutorial paper is to provide a qualitative description of acoustic streaming and an appreciation of the ways in which streaming can be harnessed for useful applications. A more theoretical approach to acoustic streaming is provided in parts 13, 15 and 16 of this tutorial series.[6–8] The qualitative description includes illustrative examples of the different types of acoustic streaming that may arise in acoustofluidic devices. Furthermore, different microfluidic applications of each class of acoustic streaming are reviewed and discussed.

II A qualitative description of acoustic streaming

The state of the volume elements of a fluid, through which an acoustic wave is propagating, is described by pressure and velocity oscillations. In an ideal fluid, the time-averaged particle displacement, *i.e.* the net fluid flow, is zero everywhere. However, in real fluids the viscous attenuation results in the net displacement of fluid particles during each cycle of oscillation becoming non-zero. This local effect may lead to a global formation of streaming flows.[9] Thus, acoustic streaming is a steady fluid flow formed by viscous attenuation of an acoustic wave.[10] Lighthill[1] used this concept in order to derive a Navier–Stokes based equation describing acoustic streaming as a non-oscillatory Reynolds stress (*i.e.* a time-averaged momentum flux in a fluid) generated by the presence of a spatial gradient in the oscillatory Reynolds stress. For the governing equations of acoustic streaming, we refer to the book chapter written by Nyborg,[11] or to parts 13, 15 and 16 in this tutorial series.[6–8]

Streaming flows vary greatly depending on the mechanism behind the attenuation of the acoustic wave. The variations include the velocity of the flow, the length scale of the flow and the geometry of the flow. The velocity varies from being on the order of $\mu m\ s^{-1}$ in the case of slow streaming, up to velocities on the order of $cm\ s^{-1}$ or more in the case of fast streaming.[12] The length scale varies from being on the order of μm in the case of microstreaming up to the order of cm in bulk-streaming.[12] The flow geometry may take the form of a jet or of vortices.[12] The above scales are not definitive but rather the scale at which streaming is most commonly observed. They are, therefore, a reflection on the frequencies and acoustic intensities adopted by researchers more than they are a reflection on what is possible. Within this section, inner and outer boundary layer streaming, Eckart streaming and cavitation microstreaming are reviewed to provide the reader with a grasp of the streaming flows that can be generated by the viscous attenuation of an acoustic wave.

A Inner and outer boundary layer acoustic streaming

Boundary layer driven acoustic streaming is formed by the viscous dissipation of acoustic energy into the boundary layer of a fluid along any solid boundary that is comparable or greater in length (in the direction of acoustic propagation) than a quarter of the acoustic wavelength.[13] Furthermore, the streaming flow is typically observed in fluid cavities where at least one dimension perpendicular to the direction of acoustic propagation is comparable in size to the acoustic wavelength.

The dissipation into the boundary layer is comparatively large in comparison to bulk dissipation because of the steep velocity gradient that is formed perpendicular to the solid boundary as the acoustic wave propagates parallel to it, see Fig. 1. The cause of the steep gradient is the presence of a non-slip boundary between the solid surface and the fluid. This results in an acoustic velocity that varies from zero at the solid surface, to its freestream value at a

Roy Green

Roy Green received his B.Eng. degree in mechanical engineering from the University of Southampton, UK, in 2009. He is currently working towards his PhD degree within the electromechanical research group of the School of Engineering Sciences at the University of Southampton under the supervision of Dr Rosie Boltryk and Prof. Martyn Hill. Roy's doctoral research focuses on the control of cavitation microstreaming flows and on their application to biomedical research as an apparatus for subjecting the membranes of biological cells to fluidic shear stresses.

Mathias Ohlin

Mathias Ohlin received his MSc degree in Engineering Physics from the Royal Institute of Technology (KTH), Sweden, in 2009. During his studies he focused on biological physics and medical technology. He is currently pursuing his PhD degree at the department of Applied Physics at the Royal Institute of Technology in the Wiklund Group. His research is focused on ultrasonic manipulation of cells and particles within multi-well microplate devices.

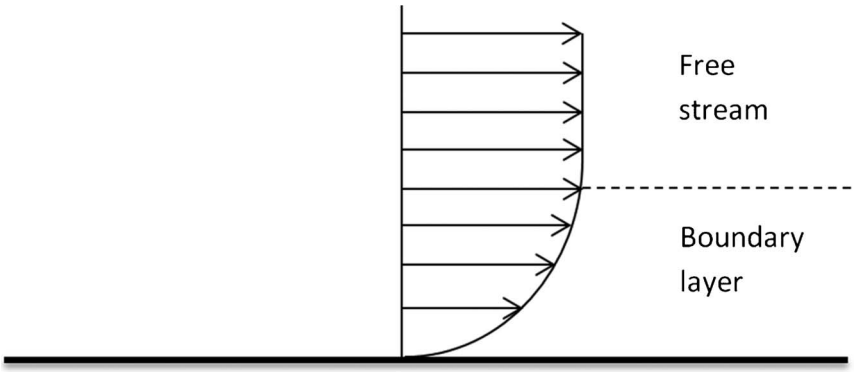

Fig. 1 Diagram showing the peak magnitude of the oscillatory first order acoustic velocity in the boundary layer. The velocity gradient is normal to the boundary and the velocity magnitude falls from its free stream value to zero. The thickness of the boundary layer in many applications is of the order of 1 μm.

distance of the order of 1 μm away from the surface (for ultrasound in water). In the case of a standing wave which is parallel to the surface, the viscous dissipation results in a steady momentum flux typically oriented from the pressure antinodes to the pressure nodes close to the solid boundary. Due to the spatially fixed pressure nodes and antinodes, this results in a steady boundary layer vorticity termed inner boundary layer streaming or 'Schlichting streaming',[14] named after Hermann Schlichting who first modelled it mathematically. Once established, the powerful inner boundary layer streaming flow then generates counter rotating streaming vortices within the bulk of the fluid accordingly named outer boundary layer streaming or 'Rayleigh streaming',[2] named after Rayleigh who first modelled them mathematically. In Fig. 2 the inner boundary (Schlichting) and outer boundary (Rayleigh) streaming are illustrated schematically. It can be seen that there is typically a vortex–antivortex pair per half wavelength along the direction of acoustic propagation. It should also be noted that when the dimension perpendicular to the boundary becomes great in comparison to the acoustic wavelength, the Rayleigh streaming vortices can become turbulent.[15]

According to Landau and Lifshitz,[16] the boundary layer driven acoustic streaming is particularly pronounced under the condition that

$$\lambda \gg h \gg \delta_v \qquad (1)$$

where λ is the wavelength, h is the characteristic length scale of the fluid chamber (*cf.* Fig. 2) and δ_v is the viscous penetration depth, which in an oscillating flow is given by[16]

$$\delta_v = \sqrt{2\nu/\omega} \qquad (2)$$

where ν is the kinematic viscosity and ω is the angular frequency of the acoustic wave. Thus, for an ultrasound wave in water in the low MHz range, λ is of the order of 1 mm and δ_v is of the order of 1 μm. This means that Rayleigh streaming is more pronounced for chambers with length scales that are fractions of a wavelength (such as the $\lambda/2$ channel typically employed in acoustophoresis). However, since the source of Rayleigh streaming in such $\lambda/2$ channels is within the boundary layer parallel to the standing wave (along x in Fig. 2), the other dimension (h, along y in Fig. 2) must also be of the order of λ or smaller to obtain significant Rayleigh streaming flows.

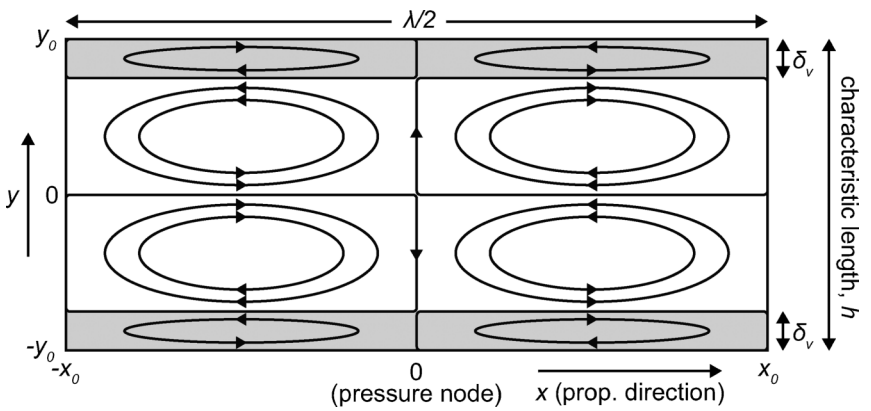

Fig. 2 A system of inner (Schlichting) streaming within the viscous boundary layer of thickness δ_v (gray areas) and outer (Rayleigh) streaming vorticies in a channel with a standing wave propagating along x. The pressure node is located at $x = 0$, which is the plane in which small particles and cells would be trapped by acoustic radiation forces. Note that the streaming is divergent within this plane and is therefore counteracting the lateral radiation force trying to aggregate suspended particles in the pressure nodal plane. The figure is based on the schematic illustration in Hamilton, Ilinskii and Zabolotskaya.[17]

When comparing the orientation of the Rayleigh streaming vortices with the position of the pressure nodes of the standing wave parallel to the boundary, the flow is in most cases divergent within the pressure nodal plane relative the central axis of the channel. This phenomenon is discussed in more detail in section III A. In Fig. 2, this corresponds to a pressure node located at $x = 0$ with its centre at $y = 0$.

Frampton, Martin and Minor[18] undertook a theoretical study in which they scaled down acoustic streaming flows to microfluidic scales. They discovered that as the size of the chamber is reduced, the inner boundary streaming becomes a larger proportion of the overall streaming flow but that the combined streaming velocity declines. Additionally, they discovered that as the acoustic frequency increases so too does the streaming velocity, though the boundary region becomes significantly smaller. They predicted a streaming velocity of over 100 μm s^{-1} in a 1 mm thick fluid channel sonicated at an acoustic pressure amplitude of 40 kPa and frequencies in the low MHz range. Their results are in agreement with the analytical solutions presented by Hamilton, Ilinskii and Zabolotskaya.[17]

B Eckart streaming

Eckart streaming, formerly called 'quartz wind', is the flow formed by the dissipation of acoustic energy into the bulk of a fluid.[19] As an acoustic wave propagates through a fluid, a proportion of the acoustic energy is absorbed by the fluid at a rate that is typically proportional to the square of its frequency (as specified in Stoke's law of sound attenuation). The amplitude of the acoustic wave becomes attenuated causing the acoustic pressure amplitude to decrease with distance from the acoustic source. The loss of acoustic energy results in a steady momentum flux, forming a jet of fluid inside the acoustic beam in the direction of acoustic propagation. For the case of a fluid jet formed within the confinement of a microfluidic chamber, vorticity will typically ensue, resulting in fluid circulation within either part of or within the entire chamber (see Fig. 3).

Matsuda, Kamakura and Maezawa[20] used Doppler velocimetry to measure the velocity of an Eckart streaming jet in water generated by a focused ultrasonic transducer operated at a pressure amplitude of 40 kPa and a frequency of 3.45 MHz. The fluid jet was approximately 1 cm in diameter and had a maximum velocity in excess of 6 cm s^{-1}. Along the radial axis the velocity was greatest at the centre of the jet whilst axially the velocity peaked at approximately 60 mm from the transducer surface, beyond which the velocity became attenuated. Cosgrove *et al.*[21] reported flow velocities of up to 5 cm s^{-1} and a jet length of 10 cm when sonicating water at an acoustic pressure amplitude of 300 kPa and a frequency of 3.5 MHz. They reported radial and axial distributions of flow velocity that mirror those reported by Matsuda, Kamakura and Maezawa.[20] It has been stated by Squires and Quake[22] that in order to generate significant Eckart streaming the chamber dimension that forms the length through which the acoustic wave propagates must be comparable to or greater in length than the acoustic attenuation length. They state that this length is 8.3 mm in water at 50 MHz and that it is inversely proportionate to the square of the frequency. Thus, Eckart streaming will only take place in microfluidics devices when high frequency ultrasound is propagated along a dimension on the order of a millimeter or longer. Eckart streaming can be generated in both standing and travelling waves though it will occur at much lower velocities in the former because the steady Reynolds stress will be generated in opposing directions, partially cancelling itself out.

C Cavitation microstreaming

Cavitation microstreaming is the flow formed by the viscous dissipation of acoustic energy in the boundary layer of a stably oscillating microbubble,[23] an altogether different concept from that of a fluid jet formed by the destructive cavitation of a bubble, which despite being an acoustically induced flow is not a form of acoustic streaming. The factor that sets cavitation microstreaming apart from other forms of boundary layer induced streaming is that the forced oscillation of microbubbles, sonicated at or near their resonance frequencies, results in the local amplification of the first order velocity.[13] It is this high amplitude bubble scattered acoustic field from which the cavitation microstreaming flows are generated.[11] The additional acoustic loss generated results in comparatively high velocity streaming flows, several orders of magnitude larger than the streaming velocity around similar sized solid particles. There are numerous modes of bubble oscillations and therefore no single flow pattern for cavitation microstreaming. The flow pattern most often associated with an unconfined gas bubble undergoing spherical volume oscillations is that of two toroidal vortices which when viewing in a 2-D plane through the centre of the bubble appear as 4 individual vortices. Half of such a pattern is shown in Fig. 4, taken from the well-known experiments carried

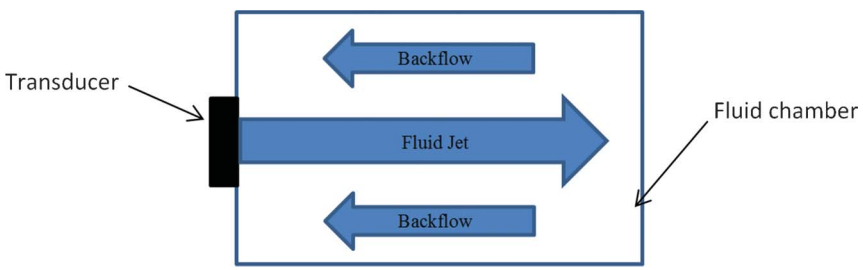

Fig. 3 A typical Eckart streaming flow including a backflow that arises due to the confined region. The fluid jet is more pronounced if the opposite wall of the chamber is acoustically absorbent and if the dimension of the fluid chamber parallel to the fluid jet is comparable or greater than the acoustic attenuation length.

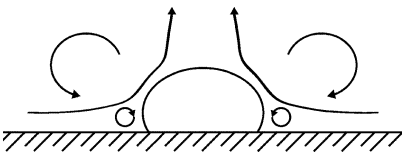

Fig. 4 Cavitation microstreaming flow around an air bubble with a surface skin, reproduced from Elder.[24]

out by Elder.[24] Here, the bubble is resting on solid boundary and therefore takes on a hemispherical shape, as a result of this only one of the two toroidal streaming vortices are formed.

The most thorough characterization of cavitation microstreaming flows carried out to date is that of Tho, Manasseh and Ooi[25] who obtained particle image velocimetry (PIV) vector fields of the flow around air bubbles of approximately 250 μm radius excited at acoustic frequencies in the range of 0.5–13 kHz in a number of different volume and translational modes whilst resting on a solid boundary for reasons of practicality. The maximum streaming velocities they obtained for the various modes of oscillation excited were typically on the order of 100–400 μm s^{-1}.

In practice, due to issues pertaining to the stability of air bubbles in water, encapsulated microbubbles are often used as a substitute for free air bubbles. Encapsulated microbubbles consist of a gas core, typically a fluorocarbon because of their low coefficient of diffusivity, encapsulated by a thin polymer or lipid shell thereby increasing the bubbles stability against dissolution. Using streak photography, Gormley and Wu[26] were able to estimate the microstreaming velocity in the vicinity of Albunex encapsulated microbubbles (1–10 μm radius) to be in the range of 50–100 μm s^{-1}, with sonication carried out at an acoustic pressure amplitude of 500 kPa and a frequency of 160 kHz. Noteworthy is the fact that the driving frequency of 160 kHz is significantly lower than the resonance frequency of Albunex, estimated to lie in the region of 800 kHz. It has been predicted through numerical calculations carried out by Doinikov and Bouakaz[27] that higher velocity streaming flows can be generated by microbubbles encapsulated by thinner and lower stiffness shells because such microbubbles will oscillate with higher amplitudes.

III Microfluidic applications of acoustic streaming

In this section we review different microfluidic applications and the observed consequences of acoustic streaming. The applications are classified into Rayleigh streaming, Eckart streaming, cavitation microstreaming and surface acoustic wave induced streaming.

A Applications of Rayleigh streaming

Rayleigh streaming has been discussed extensively within the field of acoustic particle trapping and manipulation, primarily in half-wave chambers. The main reason is that streaming places a practical lower limit on the particle size that can be manipulated by the primary radiation force in a standing wave. This is particularly relevant when the streaming direction is opposite to the direction of the radiation force. The first thorough microscopic studies were carried out by Spengler *et al.*,[28,29] who investigated the effect of Rayleigh streaming on the agglomeration of yeast cells and polymer beads with sizes ranging from 1 to 25 μm. They studied the lateral motion of the particles within the pressure nodal plane in a half wavelength standing wave device with an acoustic pressure amplitude of 500 kPa and a frequency of around 3 MHz. They observed that whilst larger (> 10 μm) particles became agglomerated in the centre of the pressure nodal plane, the 1 μm particles did not because the drag from the streaming flow overcame the lateral radiation force, see Fig. 5.

It can be seen in Fig. 5a that the orientation of the Rayleigh streaming within the pressure nodal plane is divergent, which is in agreement with the streaming orientation in the corresponding plane (x = 0) in the schematic illustration in Fig. 1. The 1 μm beads were not noticeably affected by the lateral radiation force and can therefore be used as flow tracers. On the other hand, the trapping and aggregation of 25 μm beads did not seem to be influenced by the counteracting streaming flow within the pressure nodal plane (see Fig. 5b). However, Spengler, Coakley and Christensen[28] observed an interesting behaviour of intermediate sized beads (which, in their work was 10 μm). Their observation, as seen in Fig. 6, was that the beads were only able to overcome the drag from the Rayleigh streaming after they formed mini-aggregates off-axis at the edges of the acoustic field. Thus, although the final result is the formation of a large aggregate in the centre of the pressure nodal plane, the process began with a depletion of beads in that plane. Spengler, Coakley and Christensen[28] explained that this was

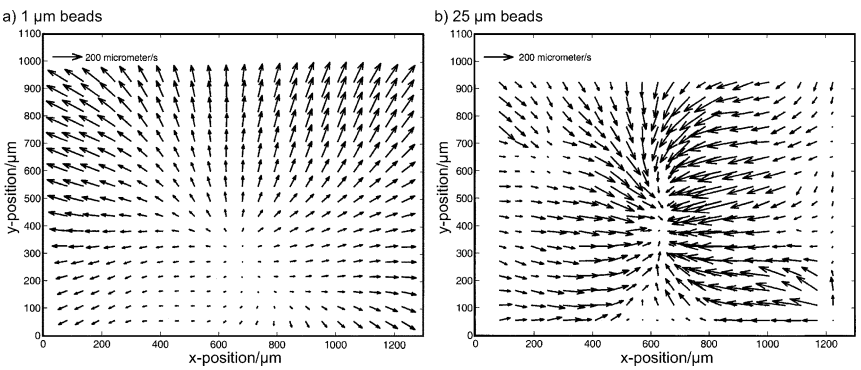

Fig. 5 Particle image velocimetry (PIV) analysis of the lateral motion of (a) 1 μm beads and (b) 25 μm beads within the pressure nodal plane (500 kPa pressure amplitude). The diagrams are taken from Spengler, Coakley and Christensen.[28]

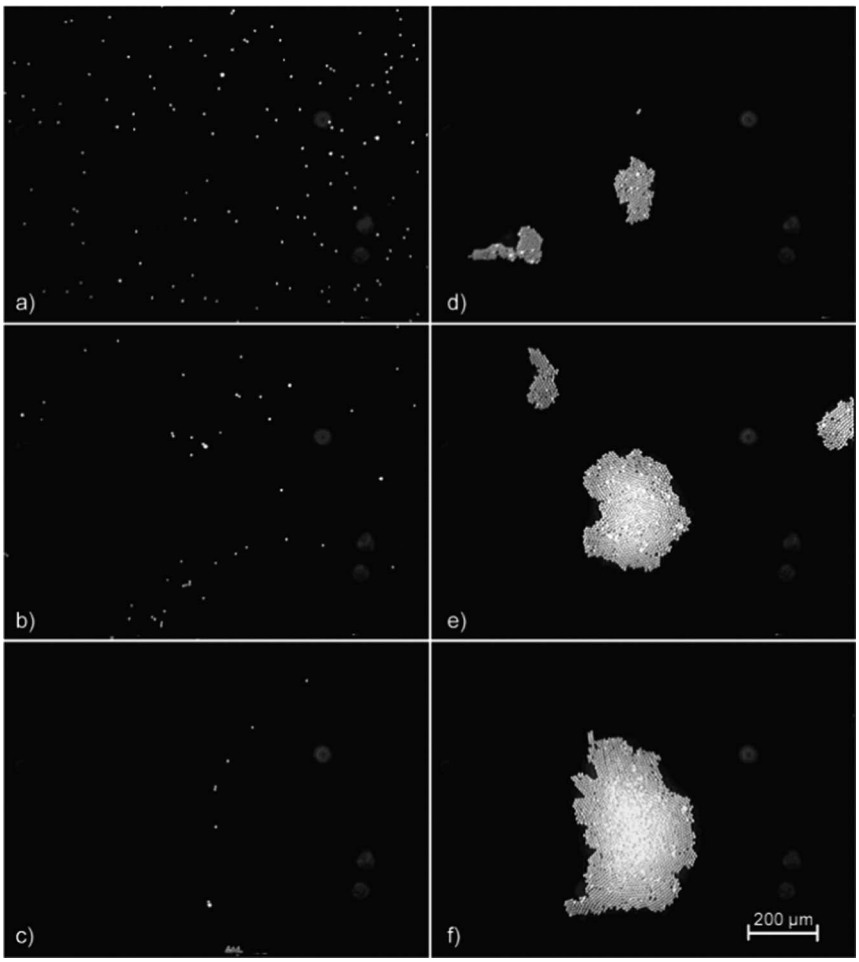

Fig. 6 In-plane development of an aggregate of 10 μm polymer beads at times (a) 0.2 s, (b) 5 s, (c) 15 s, (d) 60 s, (e) 130 s, and (f) 190 s. Once driven to the pressure nodal plane, the beads initially move away from the center of the field of view due to Rayleigh streaming (a–c). They interact off camera and return as compact mini-aggregates (d–e). The packing of the growing central aggregate adjusts to incorporate these merging mini-aggregates (f). The figure is taken from Spengler and Coakley.[29]

caused by the increase of the effective volume of the mini-aggregates relative to single beads. Thus, the increase in effective volume has a stronger effect on the volume-dependent radiation force than on the radius-dependent viscous drag from acoustic streaming.

Kuznetsova and Coakley[30] generated and measured Rayleigh streaming in circular and rectangular water filled acoustic chambers of varying thicknesses sonicated at acoustic frequencies of 1.5–3 MHz in order to setup either quarter or half wavelength standing wave resonances with pressure amplitudes in the range of 310–600 kPa. The maximum streaming velocities measured for each setup ranged from below 100 μm s^{-1} to approximately 500 μm s^{-1}. In agreement with Frampton, Martin and Minor,[18] they found that increasing either the frequency or pressure amplitude resulted in a considerable increase in the streaming velocity, whilst halving the chamber thickness so as to obtain a quarter wavelength resonance had the effect of reducing the streaming velocity. By careful device design, Kuznetsova, Martin and Coakley showed that the radiation force may dominate over streaming for 1 μm particles.[30] Comparing the results of Spengler *et al.*[28,29] and Kuznetsova *et al.*,[30,31] it is obvious that the streaming direction relative the radiation forces has important consequences on the ability to trap small particles. It should also be mentioned that the fluid chambers used by both Spengler *et al.*[28,29] and Kuznetsova *et al.*[30,31] had lateral dimensions (h) that did not fulfil the relationship in eqn (1). Instead, h was typically much larger than λ in their devices. This indicates that the source of Rayleigh streaming is most likely not solely located in the boundary layers parallel with the standing wave direction (*i.e.* parallel to x in Fig. 2). A possible explanation is that flexural vibrations in the carrier and reflector layers in the $\lambda/2$ chambers generate streaming also in the boundary layers perpendicular to the standing wave direction (*i.e.* parallel to y in Fig. 2).

Bengtsson and Laurell[32] used Rayleigh streaming for efficient fluid mixing and stirring in resonant microchannels. They evaluated two different systems: one device for fluid mixing of two parallel flows in a single channel, and one device for fluid stirring in order to increase enzymatic reactions taking place on the chamber walls in a 32-channel microstructure. Both devices had channel heights corresponding to a full wavelength (300 μm at the driving frequency of ~ 5 MHz). The channel width

corresponded to a quarter of a wavelength in the mixing device (75 μm), and even less (25 μm) in the 32-channel enzyme reactor. Interestingly, the mixing device had a very narrow frequency bandwidth, while the enzyme reactor was more broadbanded. In the latter device, the catalytic effect increased by 20% when ultrasound was applied, as compared to the controls.

A more detailed analysis of the size-dependent cross-over from radiation force dominance (large particles) to streaming dominance (small particles) was carried out by Barnkob *et al.*[33] who used experimental data of bead motion in a theoretical model to estimate the relative weight of the radiation force and the streaming force, respectively. Their theoretical model is based on the decomposition of the particles velocity field into a gradient part and a rotation part, in order to derive the (gradient-type) radiation force and (rotation-type) acoustic streaming contributions to the overall particle motion. They concluded that the theoretical threshold, defined as the particle size for which the two forces were equal in magnitude, corresponded to a particle with a diameter of 2.6 μm at the driving frequency 2 MHz, and that the threshold particle size is proportional to $1/\sqrt{f}$, where f is the driving frequency. This is in agreement with general experimental observations, where a 2 MHz acoustophoretic device is suitable for ultrasonic manipulation of cells (which are typically larger than 3 μm)[34] and a $>$ 10 MHz device is suitable for ultrasonic manipulation of objects with sizes down to approximately 1 μm or potentially even smaller.[35] However, it should be noted that in fluid exchange applications with larger particles (typically cells with sizes $\sim$ 10 μm), acoustic streaming may decrease the wash efficiency even if the particle manipulation is not directly affected by the streaming.[34] The reason being that this type of application is dependent on both accurate displacement of the particles or cells relative the microchannel, and a retained and undisturbed laminar flow.

Several strategies have been suggested for manipulating particles smaller than the theoretical threshold defined by Barnkob *et al.*,[33] with the most important factor being the particle concentration. As seen in Fig. 6, at sufficiently high particle concentrations the acoustic particle–particle interaction force contributes to the formation of local mini-aggregates that can be manipulated due to their larger effective radius. This effect is enhanced when other particle–particle interaction forces are present such as van der Waals interactions, electrostatic interactions and hydrophobic/hydrophilic effects. Furthermore, the streaming pattern may cause a local depletion of particles from vortex regions. This is shown in Fig. 7, where a complex interaction between the direct radiation force and the acoustic streaming causes a redistribution of 400 nm polystyrene particles suspended in water in a 750 μm wide channel. At a frequency of 2.11 MHz (Fig. 7a; channel width corresponding to λ) the characteristic $\lambda/4$ scaled Rayleigh streaming vortices are clearly seen to cause a local depletion of particles within each vortex. Here, the global effect is a decrease in particle concentration along the centre of the channel. This effect becomes more pronounced at a frequency of 6.62 MHz (Fig. 7b; channel width corresponding to 3λ) where the radiation force appears to

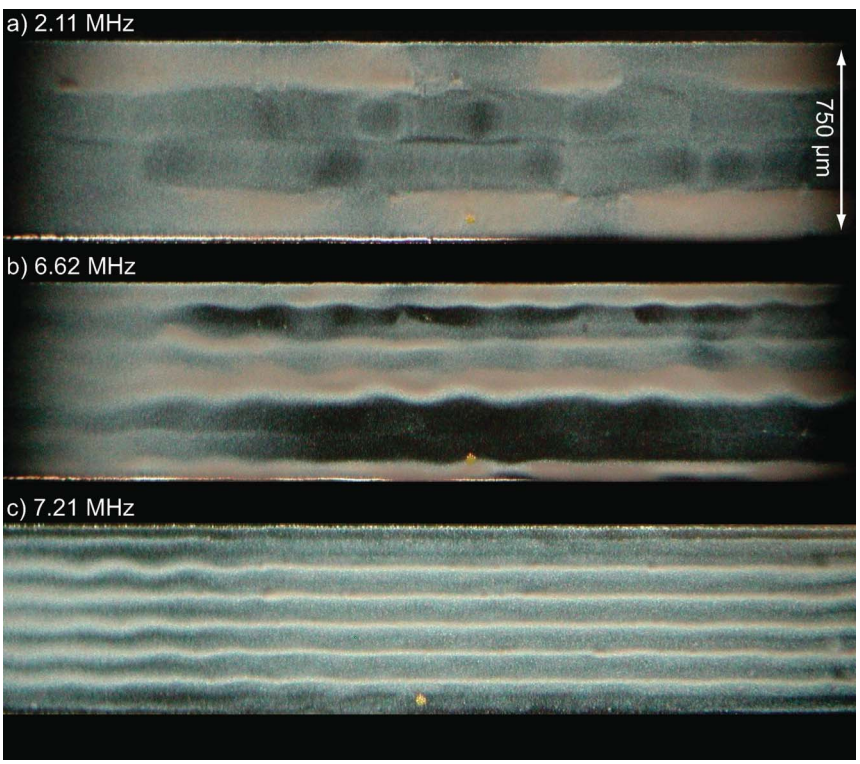

Fig. 7 The redistribution of highly concentrated 400 nm polystyrene particles suspended in water in a 750 μm wide channel due to the interaction between the direct radiation force and acoustic streaming. As seen in the images, the influence of acoustic streaming decreases with frequency. The driving voltage is 7 V_{rms} and the frequency is (a) 2.11 MHz, (b) 6.62 MHz and (c) 7.21 MHz. Experiments by Martin Wiklund.

be more significant than at 2.11 MHz. At 7.21 MHz (Fig. 7c; channel width corresponding to 3.5λ), the pattern of aligned particles is in agreement with standard acoustophoretic operation (*i.e.* $\lambda/2$ distance between nodes) and there is no clear evidence of Rayleigh streaming vorticity. The experiments in Fig. 7 demonstrate that it should be possible to design systems where acoustic streaming enhances rather than inhibits the desired particle manipulation in a standing wave manipulation device. Other strategies for sub-μm particle manipulation include the use of surface acoustic wave (SAW) devices compatible with higher frequencies (typically 20–40 MHz),[36] or the use of larger (>μm) seeding particles to trigger attractive particle–particle interaction forces between an aggregate of seeding particles and individual sub-μm particles.[37] The latter is a recently reported development and a very attractive method with which nanoparticles at low concentration may also be agglomerated by ultrasound.

The orientation and size of the streaming vortices have been a matter of debate. The reason is that the predicted standard orientation of the rotational flows based on boundary layer losses in simple geometries (*cf.* Fig. 2 and Fig. 7a) is not always confirmed experimentally. In some cases the Rayleigh streaming vortices may rotate in the opposite direction to that expected, and/or they can be of $\lambda/2$ size rather than of $\lambda/4$ size. Examples of this include the 6×6 array of Rayleigh vortices observed in a $3\lambda \times 3\lambda$ chamber,[38] and the $1 \times n$ array of Rayleigh vortices in a $\lambda/2$ wide microchannel,[39] see Fig. 8. A suggested explanation for this phenomenon is the hypothesis that not only losses in the viscous boundary layer, but also transmission losses in the solid structure of an acoustophoretic chip, contribute to the total acoustic streaming.[40] Thus, while the ultrasound resonance modes in an acoustophoresis chip can be modelled in good agreement with experimental observations by only considering the channel geometry,[41] quantitative acoustic streaming modelling requires that the entire chip, including the solid structures surrounding the channel, are incorporated into the model. Another possible explanation is the contribution of flexural vibrations in the solid structure facing the fluid chamber to the losses in the viscous boundary layer.

In addition to the boundary conditions and loss mechanisms involved, the geometry of a microchannel or microchamber has a large impact on the magnitude and geometry of acoustic streaming. Experimental examples of the acoustic streaming observed in micro-scaled resonance cavities of different geometries are shown in Fig. 9. The characteristic $\sim \lambda/4$ scaled Rayleigh streaming vortices are seen in a circular (Fig. 9a) and square (Fig. 9b) shaped chambers inside a flow-through chip, while a single $\lambda/2$ scaled vortex is seen in one well of a 100-well micro-plate (Fig. 9c). Finally, a well with sharp edges can be used for generating well-localized streaming vortices originating from the tip of the sharp structure (Fig. 9d). This effect is well-known in acoustophoresis chips having a branched channel outlet. Thus, sharp edges should be avoided in applications where streaming must be minimized. On the other hand, the device in Fig. 9d can be used for fluid stirring in the vicinity of trapped particles or cells.[42] In summary, Fig. 9 demonstrates the complexity of acoustic streaming in microfluidic devices and gives an indication of the difficulties to accurately model and predict the streaming.

An interesting method for controlling acoustic streaming inside multi-well plates designed for cell trapping is to use a frequency modulation based driving scheme.[43] This method is based on the fact that each single-frequency operation of the device shown in Fig. 9c causes a $\lambda/2$ scaled vortex with either clockwise or counter clockwise orientation. By sweeping the frequency within a suitably selected bandwidth, the net effect causes the streaming to be heavily suppressed without interfering with the trapping function of the device, see Fig. 10. Ohlin *et al.*[43] used this for switching on and off the acoustic streaming around a continuously trapped cell aggregate in a multi-well microplate.

B Applications of Eckart streaming

As pointed out in section II B, Eckart streaming is not the dominant form of acoustic streaming observed in microfluidics devices. The main reason for this is that boundary-layer effects dominate over bulk effects at the microscale domain, which results in Rayleigh streaming dominating over Eckart streaming. However, if the dimension of the fluid channel or chamber parallel to the propagation direction of the acoustic wave is of a scale scale > 1 mm, Eckart streaming may occur. Furthermore, if

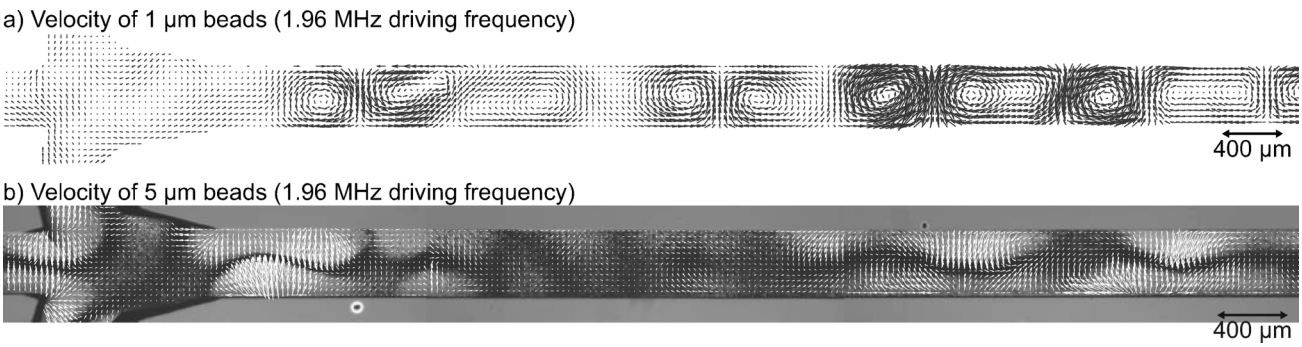

Fig. 8 (a) $\lambda/2$ scaled Rayleigh streaming vortices seen in a half wave channel driven at 1.96 MHz, tracked by particle image velocimetry (PIV) of 1 μm beads. (b) The corresponding motion of 5 μm beads at the same actuation parameters, tracked by PIV plotted on a background image showing the final distribution of beads. The streaming velocity is of the order of 10 μm s^{-1} in both experiments. The figures are combined parts from two separate figures in Hagsäter *et al.*[39]

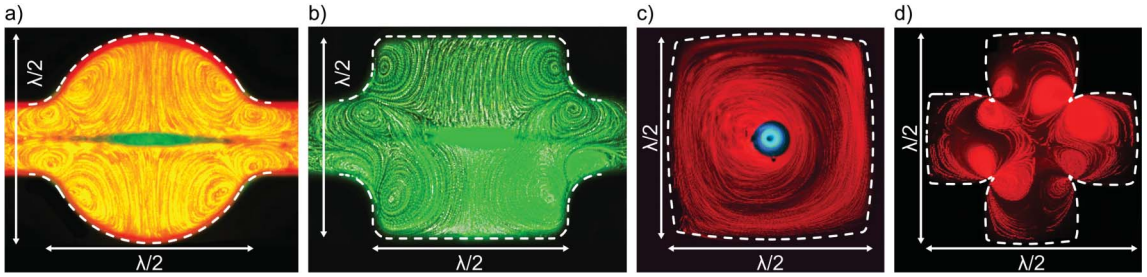

Fig. 9 Acoustic streaming patterns in different geometries of the acoustic resonant cavity, visualized by making an overlay of a series of frames from a video clip. The width is between 300 and 350 μm in all cavities, and the driving frequency is between 2.1 and 2.6 MHz. The streaming is tracked by 1 μm fluorescent beads and the trapped cluster in the centre of each cavity contains 5 μm beads in (a) and (b), and 10 μm cells in (c). There are only 1 μm beads present in (d). Experiments by Otto Manneberg (a–b) and Mathias Ohlin (c–d).

more than one dimension is of a scale > 1 mm, and if the acoustic chamber is lossy (*e.g.*, by the use of absorbing materials such as plastics), Eckart streaming is even more likely to occur.

Hertz observed Eckart streaming in an 11 MHz acoustic trap based on two counter-propagating and strongly focused waves in an $\sim 10 \times 10 \times 44$ mm^3 fluid chamber.[44] He explained the effect as the result of transducer alignment problems and mismatch in emitted beam profiles, causing a small residual propagating wave around the beam axis. In practice, Hertz eliminated this problem by the use of two acoustically transparent thin (2 μm) plastic films placed in the focal region 1.5 mm apart. The design of this pair of acoustic windows took Kolgomorov microscales in turbulent flows into account.[45]

A corresponding streaming pattern was observed by Wiklund, Hänninen and Hertz[46] in a device of similar dimension to Hertz's based on a single focusing transducer and a plane acoustic reflector, see Fig. 11. This device was developed on a 96-well plate platform with the aim of the concentration and positioning of capture beads in a bead-based immunoassay.[47] As can clearly be seen in Fig. 11, Eckart streaming can be generated over a distance of about 1 mm, resulting in fluid velocities of up to 1 mm s^{-1}. The figure displays two different orientations of Eckart streaming, either away from the transducer along the axis of symmetry when using a soft-wall reflector made of polystyrene (Fig. 11a), or towards the transducer when using a hard-wall reflector made of Molybdenum (Fig. 11b). The former orientation (Fig. 11a) is in agreement with the schematic illustration in Fig. 3. Here, the reason for the different directions is based on focusing geometry; the focal length of the transducer is longer than the fluid chamber length in both experiments. The device in Fig. 11 could be used for sweeping a fluid sample across trapped aggregates of particles confined close to the axis of symmetry of the chamber. The method has been proposed for enhancing bead-based immunoassays.[48]

Möller *et al.* recently investigated both theoretically and experimentally the orientation of Eckart streaming in a 1 mL (11.5 mm long) plastic chamber for two different actuation frequencies.[49] They noticed that a 6.5 MHz actuation frequency resulted in a forward-directed axial flow and a peripheral backflow (similar to the directions in Fig. 3 and Fig. 11a), while a 2 MHz actuation resulted in an oppositely directed flow pattern (similar to the direction in Fig. 11b). They demonstrated that their experimental observations were in good agreement with a theoretical model that included the piezoelectric behaviour of the transducer and the structural mechanics of the PMMA chamber as well as the fluid domain. They explained the effect of the reversed direction for the lower frequency as a result of radiation

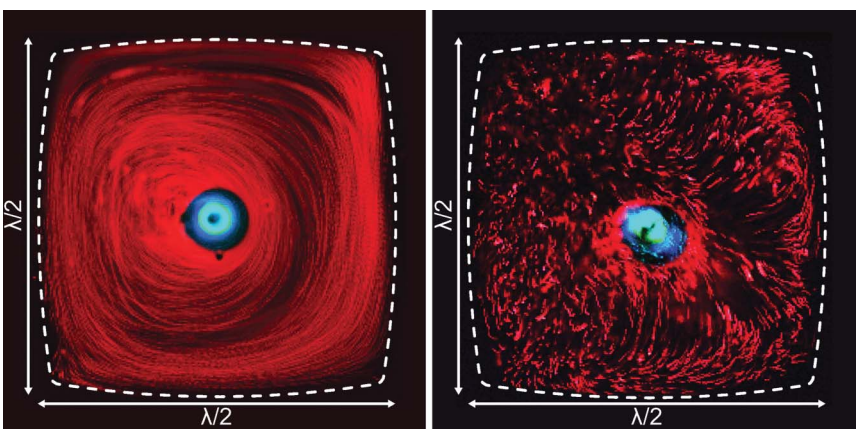

Fig. 10 Demonstration of the acoustic streaming obtained at single frequency (left) and frequency modulation (right) actuation inside one 350 μm wide well in a multi-well microplate. The left image is an identical flow to Fig. 8c. The frequency modulation method decreases the acoustic streaming by a factor ~ 30 without effecting the positioning of the cluster of 10 μm particles in the centre of the well (blue cluster) by acoustic radiation forces. Further experimental details are found in Ohlin *et al.*[43]

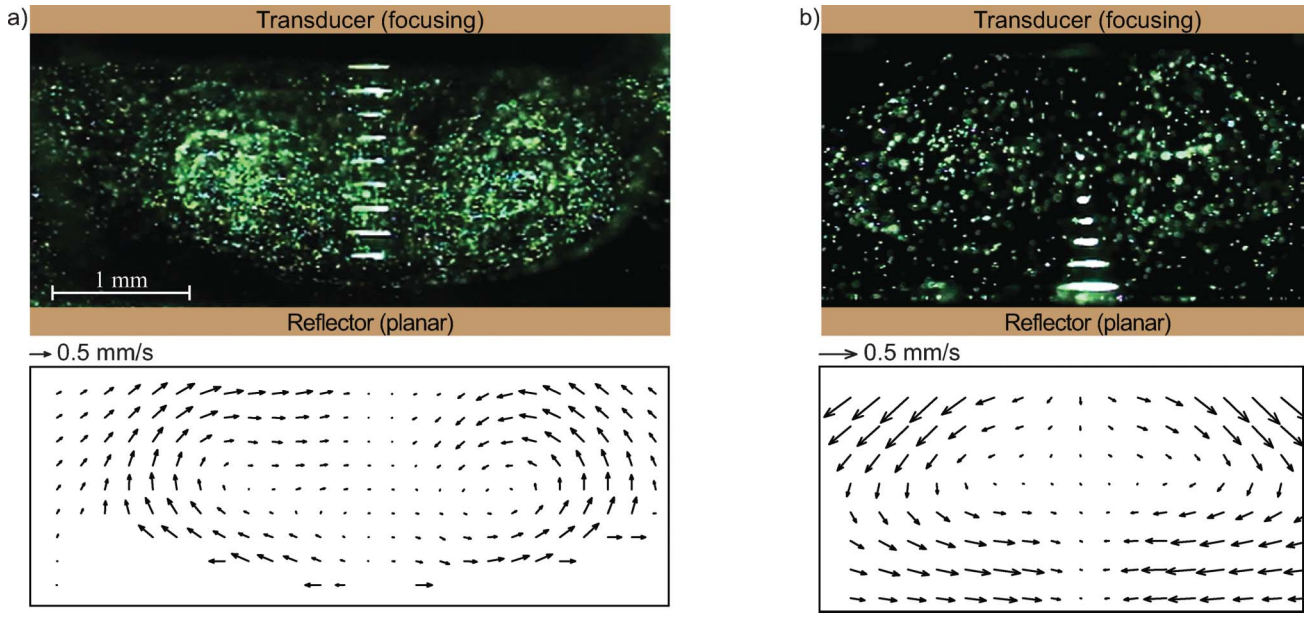

Fig. 11 Eckart streaming generated between a focusing 4-MHz ultrasound transducer and a plane reflector made of polystyrene (a) and molybdenum (b). The upper panel shows experimental side-view snapshots of 4 μm fluorescent beads suspended in water, and the lower panel shows corresponding velocity fields from PIV analysis. Along the symmetry axis, ultrasonic trapping of 4 μm particles in several pressure nodes are seen. Further experimental details are found in Wiklund, Hänninen and Hertz.[46]

taking place from the whole PMMA structure and not only from the transducer, resulting in a complicated acoustic field inside the chamber. The suggested application of the device was in purification processes if combined with a particle trap.

C Applications of cavitation microstreaming

Cavitation microstreaming flows formed in the vicinity of oscillating microbubbles are of extremely high velocity in comparison to streaming flows formed in the vicinity of non-compressible spheres of a similar size. Depending on the acoustic pressure and the size of the microbubble it is possible to achieve flow circulation over a wide range of scales from nanolitre up to millilitre volumes. As a consequence of the wide range of scales cavitation microstreaming is applicable both to the generation of whole scale flows and to the generation of highly targeted flows. The two applications of cavitation microstreaming that have received the most attention are micro mixing and cell membrane poration; these are discussed within this paper alongside several novel applications.

Wang, Attinger and Moraga[50] generated cavitation microstreaming in the vicinity of a 36 μm diameter air bubble and used the flow to drive a self-aligning rotor of similar size. By modifying the acoustic frequency they were able to drive the rotor at varying speeds, achieving a maximum angular speed of over 700 rpm. Although the power output of the rotor was estimated to lie in the femtoWatt range, its power density was 100 MW m^{-3}. Further work has shown that there exists a linear relationship between the driving voltage of the transducer and the rotational speed of the rotor.[51] The authors have not discussed what the possible applications of the micro-rotor may be though presumably they could include pumping, centrifuging and even micro propulsion. In addition to the high energy density achieved, the advantage of a bubble driven micro-rotor is the absence of the need for a physical connection to a power supply.

Pumping of fluid is vital for many microfluidics applications. Due to the vorticity of the flow in cavitation microstreaming, it has received little attention as a method for micro pumping. This is despite the fact that unlike many other pumping technologies it does not rely on the chemical/ionic composition of the fluid or on complex channel geometries. In one example of pumping, Ryu, Chung and Cho[52] generated a maximum flow velocity of 5.3 mm s^{-1} and a corresponding flow rate of 0.19 mL s^{-1} with a pressure load of 253 Pa in a 300 μm diameter capillary. This was achieved by fixing a capillary tube directly above a 400 μm in diameter oscillating air bubble so as to direct a proportion of the flow into the capillary. The experimental setup can be seen in Fig. 12. Additionally, Marmottant and Hilgenfeldt[53] have demonstrated that by using a bubble–particle doublet, microstreaming flows can be generated with a directional component that can be used to transport cells.

An additional highly promising application of cavitation microstreaming is the mixing of minute volumes of fluid. Impeded by the low Reynolds number, mixing in microfluidics poses a technical challenge but is vital in order to ensure fluid homogeneity, increase rates of chemical reaction and for heat transfer. Although cavitation micro-streaming is by no means the only effective means of mixing fluids in microfluidics, it has been demonstrated in numerous research papers to be an extremely rapid method for mixing fluids in microchannels.

The microbubbles that generate the microstreaming flows are typically formed by trapping air in hydrophobic grooves cut into the sides of fluidic

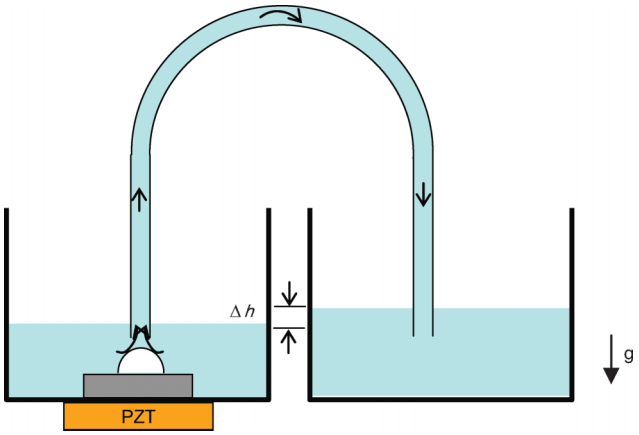

Fig. 12 A schematic of the experimental setup for a single bubble micro-pump by Ryu, Chung and Cho[52] A 400 μm diameter air bubble is excited acoustically in order to generate microstreaming flow that drives a flow of 0.19 mL s^{-1} through a 300 μm diameter capillary.

channels. The cavitation microstreaming flows that form upon ultrasonic excitation have been shown to lead to the complete mixing of fluids within several microseconds in flow-through devices with flow rates in excess of 10 μL min^{-1}.[54] Within static fluid volumes, it has been demonstrated that a 50 μL volume can be mixed in 6 s.[55] Taking one particular example from the literature, as shown in Fig. 13, a horseshoe shaped feature was used to trap air inside the microfluidics device so as to mix two laminar flows as they combine inside a larger channel with a cross-section of 240 μm × 155 μm. It was reported in the paper that at a flow rate of 8 μL min^{-1}, the flow velocity past the horseshoe feature was 7.2 mm s^{-1} (without mixing) and that at this velocity the two laminar flows became completely mixed within a 50 μm distance from the start of the mixing region, a distance that takes the fluid 7 ms to transverse at the reported velocity. An alternative design based on the same concept was presented by Tovar and Lee[56] who called their device a lateral cavity acoustic transducer. This device was capable of pumping or mixing fluids in a microchannel at a flow rate of approximately 250 nL min^{-1}. Recently, the technique has been used for switching cells or particles into bifurcating microchannels,[57] and pumping at the pressure of 350 Pa (at 25 V_{pp} and 35 kHz actuation voltage).[58]

Further demonstrations of cavitation microstreaming enhanced micro-mixing include the 5 fold increase in the rate of DNA hybridisation that would otherwise be severely limited by the time taken for diffusion to occur.[55] Despite the high success of many of the devices reported in the literature, there do not appear to be any commercial cavitation microstreaming based micro-mixers on the market to date.

The final application of cavitation microstreaming to be discussed is its application to biomedical research. It has been demonstrated that the shear force exerted by microstreaming flows on the cellular membrane of biological cells may result in significant physiological effects. These effects, described in more detail by Wiklund,[59] include but are not limited to, an increase in cell metabolism,[60] cellular differentiation,[61] the elongation endothelial cells[62] and cellular membrane poration.[63] It is in fact possible to generate sufficient shear stress to lyse cells, for instance Rooney[64] demonstrated that microstreaming generated by air bubbles is sufficient to cause hemolysis of erythrocytes. In the vast majority of studies into the generation of shear stress on cell membranes, acoustic contrast agents such as Optison and Albunex have been used instead of free air bubbles. The rationale for their use is

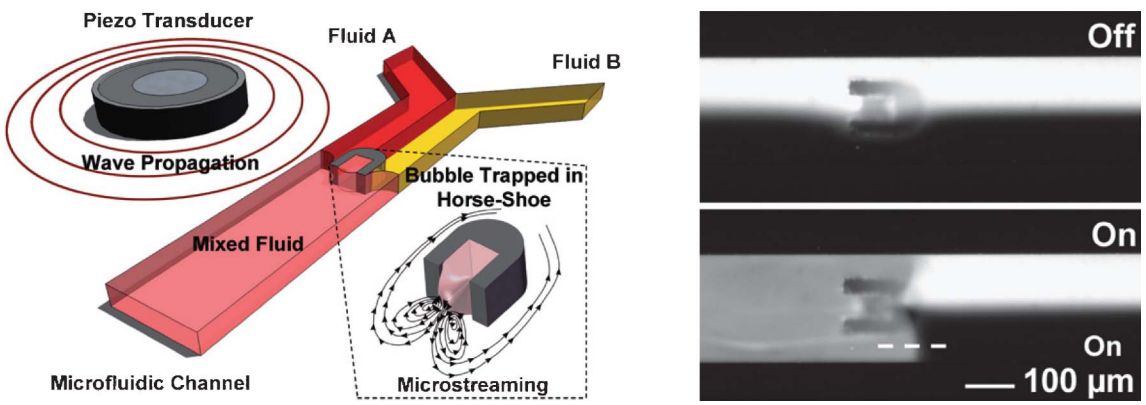

Fig. 13 A schematic of the experimental setup of Ahmed *et al.*[53] for acoustic streaming generated at a microbubble trapped inside a horseshoe-shaped structure (left) and a demonstration of the device by mixing a flow of water and a fluorescent dye solution (right). The flow in going from right to left. The figure is based on two separate figures from ref. 53.

that they are more stable, smaller and can be more easily targeted to cells.

Of the aforementioned physiological effects on cells, it is the use of shear stress to permeabilize the cell membrane that has received the greatest attention. Much of the research has involved the use of inertial cavitation, an extremely violent event that leads to high levels of cell lysis.[65] In the largest proportion of the research carried out to date the authors have failed to make a distinction between stable and inertial cavitation and so poration is likely to occur as a result of both forms of cavitation, of which inertial cavitation is not considered to be a microstreaming flow. In a study carried out by Bao, Thrall and Miller,[66] it was reported that almost 40% of Chinese hamster ovary cells took up FITC-dextran when sonicated at 0.8 MPa in the presence of Albunex contrast agent, compared to 0% in their controls, however no test was carried out to probe for the presence of inertial cavitation.

Several studies carried out have demonstrated that the magnitude of shear stress generated during cavitation microstreaming is applicable to cellular poration. In one such study, a PZT transducer fixed to the back of a Mason horn was used to generate a streaming flow of similar magnitude to a typical cavitation microstreaming flow.[67] The rationale for the use of the Mason horn was that it would allow for the spacing between the horn tip and the cells to be easily determined and that there would be scant chance of inadvertently generating inertial cavitation. By utilising theoretical models in combination with the experimental data, it was estimated that a threshold shear stress of 12 Pa is required to porate the cellular membrane, a figure that has been advocated by additional researchers.[68–70]

Marmottant and Hilgenfeldt[71] have predicted that the vessel lysis of giant unilaminar lipid vesicles by stable cavitation of free air bubbles 10–100 μm in radius, excited at an acoustic frequency of 180 kHz may occur at a pressure amplitude as low as 10 kPa in a high viscosity liquid. Their prediction was made by calculating the increase in shear stress that would occur as a result of a 20 fold increase in the viscosity of water.

D Surface acoustic wave induced streaming applications

It has been demonstrated that acoustic streaming generated by surface acoustic waves (SAWs) has numerous important applications in microfluidics. SAW streaming is not easily classified as either boundary-layer driven or bulk driven streaming, and is therefore discussed separately. The SAW, initiated by an interdigitated transducer (IDT), forms a pressure wave inside a fluid compartment, such as a droplet, in which acoustic streaming is generated by viscous attenuation.[72] At low acoustic amplitudes the phenomenon has been utilised for rapid mixing within a droplet. Wixforth[73] had demonstrated that a fluorescent dye can be mixed with a 50 nL droplet of water in under a second. At high acoustic amplitudes the steady momentum flux generated is able to displace the droplet, a phenomenon that has been utilised for the formation and actuation of micro droplets. The technique is also applicable to mixing in microtiter plates, see Fig. 14. This device has been commercialized under the name PlateBooster™ by Beckman Coulter (formerly by Advalytix).

Using a similar device as Wixforth's,[73] Luong, Phan and Nguyen[74] reported that high actuation voltages of an acoustic micromixer could lead to significant heating. For example, using actuation voltages in the interval 35–75 V resulted in a maximum temperature in the range ~ 30–70 °C. Similar results have previously been reported by Tseng *et al.*[75]

In a microfluidic device created by Franke *et al.*[76] (Fig. 15), water droplets of 20 μm in diameter could be displaced away from an interdigitated transducer (IDT), providing control over which outlet channel the droplets enter. In a follow-up of this work, cell sorting was demonstrated at the impressive rate of several kHz.[77] In another experiment it was shown that a water droplet linear actuation velocity of 12 mm s^{-1} could be achieved as long as the acoustic wavelength is smaller than the diameter of the droplets.[78]

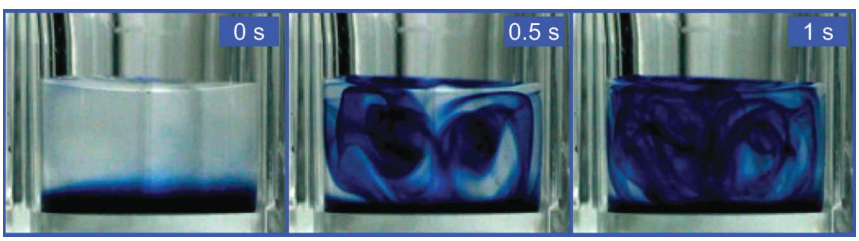

Fig. 14 Surface acoustic wave (SAW) induced mixing in one well in a 96-well plate. The well diameter is approx. 6 mm. Figure taken from Wixforth.[73]

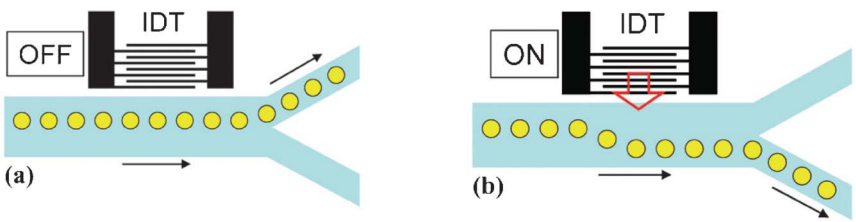

Fig. 15 A surface acoustic wave used to deflect water droplets. Figure is taken from ref. 76.

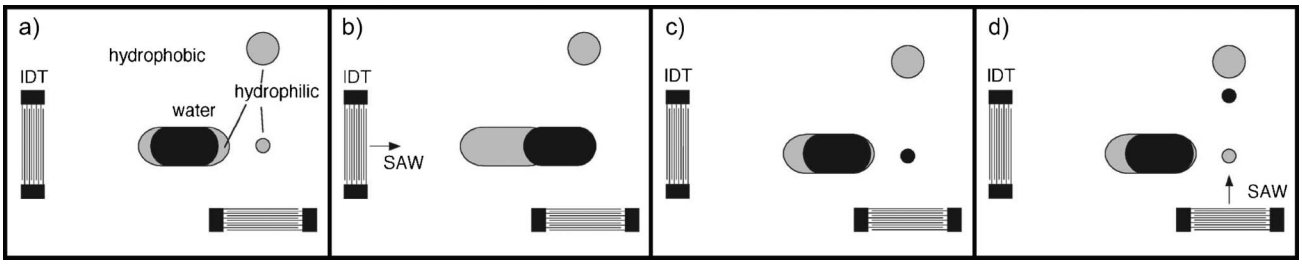

Fig. 16 "Device for forming precise water droplets based on two crossing SAWs. (a) Initial position with a large, water filled hydrophilic anchor site and an empty small one. (b) Left-right propagating SAW pushes large water droplet onto the small anchor site. (c) After turning off the SAW, the large water droplet relaxes back to its initial position, leaving the small anchor site filled with a precise minute quantity of water. (d) bottom-top propagating SAW pushes the small water droplet towards the output position. The figure is taken from Strobl, von Guttenberg and Wixforth.[78]

Strobl, von Guttenberg and Wixforth[78] demonstrated that the SAW induced displacement of a large fluid droplet over hydrophilic sites on an otherwise hydrophobic substrate can be used to form droplets of a precise volume. The large droplet contained within a hydrophilic reservoir site is forced over the smaller hydrophilic anchor site that defines the size of the micro droplet to be formed, see Fig. 16. Upon cessation of the SAW excitation the large droplet retracts into the reservoir leaving a precise volume of fluid over the anchor. The droplet can then be removed from the anchor. In work being discussed this is carried out by a second transducer that displaces the droplet into a third site. An advantage of using a SAW device is that a droplet can be positioned anywhere on a 2-D substrate using only 4 transducers.

IV Conclusion

Applications of acoustic streaming can be divided into methods for (1) suppressing or overcoming the streaming, and (2) methods where the streaming is actively used. The first category contains primarily methods based on cell or particle manipulation in standing wave fields. Here, the streaming typically places a practical lower limit on the particle size that can be manipulated by the acoustic radiation force. Depending on the device design, this limit is typically around 1–2 μm. An important conclusion concerning the size and orientation of acoustic streaming is that for Rayleigh streaming (the most common streaming type in microfluidic devices), the vortices are not exclusively $\lambda/4$ sized as often described in literature, but are sometimes $\lambda/2$ sized or even larger. In addition, the orientations of the vortices are often difficult to predict, although the most commonly observed orientation is according to Fig. 1. Therefore, reported experimental works need to be complemented with more accurate theoretical modelling in the future.

For the other category (2), the number of lab on a chip devices taking advantage of acoustic streaming seems to be steadily increasing. Here, applications include fluid mixing, fluid pumping, particle/cell sorting, droplet displacement, cellular membrane poration and cell lysis. Currently, this research field is very active and a few products based on acoustic streaming have already been launched commercially.

Acknowledgements

The authors are grateful for financial support by EU FP-7 RAPP-ID project (contract number 115153-2) and by the Swedish Research Council.

References

1 J. Lighthill, *J. Sound Vib.*, 1978, **61**, 391–418.
2 Lord Rayleigh, *Philos. Trans. R. Soc. London*, 1884, **175**, 1–21.
3 M. Faraday, *Philos. Trans. R. Soc. London*, 1831, **121**, 299–430.
4 E. F. F. Chladni, *Entdeckungen Über die Theorie des Klanges*, 1787.
5 V. V. Dvorak, *Ann. Physik*, 1896, **42**, 157.
6 S.S. Sadhal, Acoustofluidics 13: Analysis of acoustic streaming by perturbation methods, *Lab Chip*, 2012, DOI: 10.1039/C2LC40202E.
7 S.S. Sadhal, Acoustofluidics 15: Streaming with sound waves interacting with solid particles, *Lab Chip*, 2012, DOI: 10.1039/C2LC40243B.
8 S.S. Sadhal, Acoustofluidics 16: Acoustics streaming near liquid–gas interfaces: drops and bubbles, *Lab Chip*, 2012, DOI: 10.1039/C2LC40283A.
9 H. Feng, *Ultrasound Technologies for Food and Bioprocessing*, 2011, New York: Springer.
10 N. Riley, *Annu. Rev. Fluid Mech.*, 2001, **33**, 43–65.
11 W. L. Nyborg, *Acoustic streaming*, in *Physical Acoustics IIB*, ed. W. P. Mason, 1965, Academic Press, New York, 265–331.
12 S. Boluriaan and P. J. Morris, *Aeroacoustics*, 2003, **2**, 255–292.
13 W. L. Nyborg, *J. Acoust. Soc. Am.*, 1958, **30**, 329–339.
14 H. Schlichting, *Physikalische Zeit*, 1932, **33**, 327–335.
15 M. K. Aktas and B. Farouk, *J. Acoust. Soc. Am.*, 2004, **116**, 2822–2831.
16 L. D. Landau, E. M. Lifshitz, Fluid Mechanics, *Course of Theoretical Physics*, Vol. **6**, Butterworth-Heinemann, 2nd Ed. 2006.
17 M. F. Hamilton, Y. A. Ilinskii and E. A. Zabolotskaya, *J. Acoust. Soc. Am.*, 2003, **113**, 153–160.
18 K. D. Frampton, S. E. Martin and K. Minor, *Appl. Acoust.*, 2003, **64**, 681–692.
19 C. Eckart, *Phys. Rev.*, 1948, **73**, 68–76.
20 K. Matsuda, T. Kamakura and M. Maezawa, *Jpn. J. Appl. Phys.*, 2006, **45**, 4448–4452.
21 J. A. Cosgrove, J. M. Buick, S. D. Pye and C. A. Greated, *Ultrasonics*, 2001, **39**, 461–464.
22 T. M. Squires and S. R. Quake, *Rev. Mod. Phys.*, 2005, **77**, 977–1026.
23 X. Liu and J. Wu, *J. Acoust. Soc. Am.*, 2009, **125**, 1319–1330.
24 S. Elder, *J. Acoust. Soc. Am.*, 1959, **31**, 54–64.
25 P. Tho, R. Manasseh and A. Ooi, *J. Fluid Mech.*, 2007, **576**, 191–233.
26 G. Gormley and J. Wu, *J. Acoust. Soc. Am.*, 1998, **104**, 3115–3118.
27 A. A. Doinikov and A. Bouakaz, *J. Acoust. Soc. Am.*, 2010, **127**, 1218–1227.
28 J. F. Spengler, W. T. Coakley and K. T. Christensen, *AIChE J.*, 2003, **49**, 2773–2782.
29 J. F. Spengler and W. T. Coakley, *Langmuir*, 2003, **19**, 3635–3642.
30 L. A. Kuznetsova and W. T. Coakley, *J. Acoust. Soc. Am.*, 2004, **116**, 1956–1966.
31 L. A. Kuznetsova, S. P. Martin and W. T. Coakley, *Biosens. Bioelectron.*, 2005, **21**, 940–948.
32 M. Bengtsson and T. Laurell, *Anal. Bioanal. Chem.*, 2004, **378**, 1716–1721.
33 R. Barnkob, P. Augustsson, T. Laurell, H. Bruus, *Proc. of 14th Int.* Conference on Miniaturized Systems for Chemistry and Life Sciences (μTAS 2010), 3–7th October

2010, Groningen, The Netherlands, 1247–1249.
34 P. Augustsson, "On microchannel acoustophoresis", *Doctoral Thesis*, Lund University, 2011.
35 L. Johansson, "Acoustic manipulation of particles and fluids in microfluidic systems", *Doctoral Thesis*, Uppsala University, 2009.
36 V. Yantchev, J. Enlund, I. Katardjiev and L. Johansson, *J. Micromech. Microeng.*, 2010, **20**, 035031.
37 B. Hammarström, T. Laurell, J. Nilsson, *Proc. of 15th Int. Conference on Miniaturized Systems for Chemistry and Life Sciences (μTAS 2011)*, 2–6th October 2011, Seattle, USA, pp. 1707–1709.
38 S. M. Hagsäter, T. Glasdam Jensen, H. Bruus and J. P. Kutter, *Lab Chip*, 2007, **7**, 1336–1344.
39 S. M. Hagsäter, A. Lenshof, P. Skafte-Pedersen, J. P. Kutter, T. Laurell and H. Bruus, *Lab Chip*, 2008, **8**, 1178–1184.
40 P. Skafte-Pedersen, H. Bruus, *Proc. of 6th USWNet Conference*, Zurich, Switzerland, 13–14th November 2008.2008.
41 H. Bruus, *Lab Chip*, 2012, **12**, 20–28.
42 M. Ohlin, A. E. Christakou, T. Frisk, B. Önfelt, M. Wiklund, *Proc. of 8th USWNet Conference*, Gdansk, Poland, 4–7 September 2011.
43 M. Ohlin, A. E. Christakou, T. Frisk, B. Önfelt, M. Wiklund, *Proc. of 15th Int. Conference on Miniaturized Systems for Chemistry and Life Sciences (μTAS 2011)*, 2–6th October 2011, Seattle, USA, 1612–1614.
44 H. M. Hertz, *J. Appl. Phys.*, 1995, **78**, 4845–4849.
45 M. T. Landahl and E. Mollo-Christensen, *Turbulence and Random Processes in Fluid Mechanics*, Cambridge University Press, Cambridge, 1986, pp. 10.
46 M. Wiklund, P. Hänninen, H. M. Hertz, *Proc. of 2003 IEEE International Ultrasonics Symposium*, 5-8 October, 2003, Honolulu, Hawaii, USA.
47 M. Wiklund, J. Toivonen, M. Tirri, P. Hänninen and H. M. Hertz, *J. Appl. Phys.*, 2004, **96**, 1242–1248.
48 M. Wiklund and H. M. Hertz, *Lab Chip*, 2006, **6**, 1279–1292.
49 D. Möller, T. Hilsdorf, J. Wang, J. Dual, *Proc. of 8th USWNet Conference*, Gdansk, Poland, 4–7th September, 2011.
50 X. L. Wang, D. Attinger and F. Moraga, *Nanoscale Microscale Thermophys. Eng.*, 2006, **10**, 379–385.
51 J. Kao, X. L. Wang, J. Warren, J. Xu and D. Attinger, *J. Micromech. Microeng.*, 2007, **17**, 2454–2460.
52 K. Ryu, S. K. Chung and S. K. Cho, *JALA*, 2010, **15**, 163–171.
53 P. Marmottant and S. Hilgenfeldt, *Proc. Natl. Acad. Sci. U. S. A.*, 2006, **101**, 9523–9527.
54 D. Ahmed, X. L. Mao, J. J. Shi, B. K. Juluri and T. J. Huang, *Lab Chip*, 2009, **9**, 2738–2741.
55 R. H. Liu, R. Lenigk and P. Grodzinski, *J. Microlithogr., Microfabr., Microsyst.*, 2003, **2**, 178–184.
56 A. R. Tovar and A. P. Lee, *Lab Chip*, 2009, **9**, 41–43.
57 M. V. Patel, A. R. Tovar and A. P. Lee, *Lab Chip*, 2012, **12**, 139–145.
58 A. R. Tovar, M. V. Patel and A. P. Lee, *Microfluid. Nanofluid.*, 2011, **10**, 1269–1278.
59 M. Wiklund, Acoustofluidics 12: Biocompatibility and cell viability in microfluidic acoustic resonators, *Lab Chip*, 2012, **12**, 2018.
60 J. A. Frangos, L. V. McIntire and S. G. Eskin, *Biotechnol. Bioeng.*, 1988, **32**, 1053–1060.
61 K. Yamamoto, T. Sokabe, T. Watabe, K. Miyazono, J. K. Yamashita, S. Obi, N. Ohura, A. Matsushita, A. Kamiya and J. Ando, *Am. J. Physiol.: Heart Circ. Physiol.*, 2005, **288**, H1915–H1924.
62 M. J. Levesque and R. M. Nerem, *J. Biomech. Eng.*, 1985, **107**, 341–347.
63 D. L. Miller and J. Quddus, *Ultrasound Med. Biol.*, 2000, **26**, 661–667.
64 J. A. Rooney, *Science*, 1970, **169**, 869–71.
65 C. D. Ohl, M. Arora, R. Ikink, N. De Jong, M. Versluis, M. Delius and D. Lohse, *Biophys. J.*, 2006, **91**, 4285–4295.
66 S. Bao, B. D. Thrall and D. L. Miller, *Ultrasound Med. Biol.*, 1997, **23**, 953–959.
67 J. Wu, *Prog. Biophys. Mol. Biol.*, 2007, **93**, 363–373.
68 W. J. Greenleaf, M. E. Bolander, G. Sarkar, M. B. Goldring and J. F. Greenleaf, *Ultrasound Med. Biol.*, 1998, **24**, 587–595.
69 D. L. Miller, S. Bao and J. E. Morris, *Ultrasound Med. Biol.*, 1999, **25**, 143–149.
70 D. L. Miller and J. Quddus, *Ultrasound Med. Biol.*, 2001, **27**, 1107–1113.
71 P. Marmottant and S. Hilgenfeldt, *Nature*, 2003, **423**, 153–156.
72 K. Sritharan, C. J. Strobl, M. F. Schneider, A. Wixforth and Z. Guttenberg, *Appl. Phys. Lett.*, 2006, **88**, 054102.
73 A. Wixforth, *J. Assoc. Lab. Autom.*, 2006, **11**, 399–405.
74 T. D. Luong, V. N. Phan and N. T. Nguyen, *Microfluid. Nanofluid.*, 2011, **10**, 619–625.
75 W. K. Tseng, J. L. Lin, W. C. Sung, S. H. Chen and G. B. Lee, *J. Micromech. Microeng.*, 2006, **16**, 539–548.
76 T. Franke, A. R. Abate, D. A. Weitz and A. Wixforth, *Lab Chip*, 2009, **9**, 2625–2627.
77 T. Franke, S. Braunmüller, L. Schmid, A. Wixforth and D. A. Weitz, *Lab Chip*, 2010, **10**, 789–794.
78 C. J. Strobl, Z. von Guttenberg and A. Wixforth, *IEEE Trans. Ultrason. Ferroelectr. Freq. Control*, 2004, **51**, 1432–1436.